



This is a repository copy of *A hydrogel–fiber–hydrogel composite scaffold based on silk fibroin with the dual-delivery of oxygen and quercetin.*

White Rose Research Online URL for this paper:

<https://eprints.whiterose.ac.uk/194995/>

Version: Accepted Version

---

**Article:**

Aleemardani, M. [orcid.org/0000-0001-8261-4046](https://orcid.org/0000-0001-8261-4046), Solouk, A. [orcid.org/0000-0002-8742-1056](https://orcid.org/0000-0002-8742-1056), Akbari, S. et al. (1 more author) (2023) A hydrogel–fiber–hydrogel composite scaffold based on silk fibroin with the dual-delivery of oxygen and quercetin. *Biotechnology and Bioengineering*, 120 (1). pp. 297-311. ISSN 0006-3592

<https://doi.org/10.1002/bit.28259>

---

This is the peer reviewed version of the following article: Aleemardani, M., Solouk, A., Akbari, S., & Moeini, M. (2023). A hydrogel–fiber–hydrogel composite scaffold based on silk fibroin with the dual-delivery of oxygen and quercetin. *Biotechnology and Bioengineering*, 120, 297– 311, which has been published in final form at <https://doi.org/10.1002/bit.28259>. This article may be used for non-commercial purposes in accordance with Wiley Terms and Conditions for Use of Self-Archived Versions. This article may not be enhanced, enriched or otherwise transformed into a derivative work, without express permission from Wiley or by statutory rights under applicable legislation. Copyright notices must not be removed, obscured or modified. The article must be linked to Wiley’s version of record on Wiley Online Library and any embedding, framing or otherwise making available the article or pages thereof by third parties from platforms, services and websites other than Wiley Online Library must be prohibited.

**Reuse**

Items deposited in White Rose Research Online are protected by copyright, with all rights reserved unless indicated otherwise. They may be downloaded and/or printed for private study, or other acts as permitted by national copyright laws. The publisher or other rights holders may allow further reproduction and re-use of the full text version. This is indicated by the licence information on the White Rose Research Online record for the item.

**Takedown**

If you consider content in White Rose Research Online to be in breach of UK law, please notify us by emailing [eprints@whiterose.ac.uk](mailto:eprints@whiterose.ac.uk) including the URL of the record and the reason for the withdrawal request.



[eprints@whiterose.ac.uk](mailto:eprints@whiterose.ac.uk)  
<https://eprints.whiterose.ac.uk/>

# **A hydrogel-fiber-hydrogel composite scaffold based on silk fibroin with the dual-delivery of oxygen and quercetin**

*Mina Aleemardani<sup>1</sup>, Atefeh Solouk<sup>2</sup>, Somaye Akbari<sup>3</sup> and Mohammad Moeini<sup>2</sup>*

<sup>1</sup>Biomaterials and Tissue Engineering Group, Department of Materials Science and Engineering, Kroto Research Institute, The University of Sheffield, Sheffield S3 7HQ, UK

<sup>2</sup>Biomedical Engineering Department, Amirkabir University of Technology (Tehran Polytechnic), Tehran, Iran

<sup>3</sup>Department of Textile Engineering, Amirkabir University of Technology (Tehran Polytechnic), Tehran, Iran

## **Emails (by the order of the authors):**

[maleemardani1@sheffield.ac.uk](mailto:maleemardani1@sheffield.ac.uk), [atefeh.solouk@aut.ac.ir](mailto:atefeh.solouk@aut.ac.ir), [akbari\\_s@aut.ac.ir](mailto:akbari_s@aut.ac.ir),  
[m.moeini@aut.ac.ir](mailto:m.moeini@aut.ac.ir)

## **Corresponding author**

Atefeh Solouk, Email: [atefeh.solouk@aut.ac.ir](mailto:atefeh.solouk@aut.ac.ir), Tel/Fax: +982164545567

## **Abstract**

Supplying sufficient oxygen within the scaffolds is one of the essential hindrances in tissue engineering that can be resolved by oxygen-generating biomaterials (OGBs). Two main issues related to OGBs are controlling the oxygenation and reactive oxygen species (ROS). To address these concerns, we developed a composite scaffold entailing three layers (hydrogel-electrospun fibers-hydrogel) with antioxidant and antibacterial properties. The fibers, the middle layer, reinforced the composite structure, enhancing the mechanical strength from  $4.27\pm 0.15$  kPa to  $8.27\pm 0.25$  kPa; also, this layer is made of calcium peroxide and silk fibroin through electrospinning, which enables oxygen delivery. The first and third layers are physical silk fibroin hydrogels to control oxygen release, containing quercetin, a non-enzymatic antioxidant. This composite scaffold resulted in almost more than 40 mmHg oxygen release at least for 13 days, and compared with similar studies is in a high range. Here, quercetin was used for the first time for an OGB to scavenge the possible ROS. Quercetin delivery not only led to antioxidant activity but also stabilized oxygen release and enhanced cell viability. Based on the given results, this composite scaffold can be introduced as a safe and controllable oxygen supplier, which is promising for tissue engineering applications, particularly for bone.

**Keywords:** Oxygen-generating biomaterials; Silk fibroin; Calcium peroxide; Quercetin; Composite scaffolds.

## **1. Introduction**

Due to many reasons (e.g., trauma, disease, or even surgery), tissue malfunction or failure can happen, and grafting is a common method to treat such defects (Griffin et al., 2015). Even

though grafting is a promising technique, it has several difficulties like the limitation of organ donors, immune reactions, infections, and ethical and cultural concerns (Aleemardani et al., 2021c; Buser et al., 2016). Tissue engineering has evolved a new window to overcome these barriers (Aleemardani et al., 2021b); however, tissue-engineered scaffolds, particularly those designed for thick tissues or organs, have confronted significant challenges (i.e., insufficient oxygen and nutrients) that restrict to enter in clinics (Ashammakhi et al., 2019b; Phelps and García, 2010; Zare et al., 2021). According to the diffusion throughout the scaffold, edges have higher concentrations of oxygen and nutrients than deep regions (Vériter et al., 2013). As a result, in low oxygen level conditions (hypoxia), lactic acid fermentation as a metabolic process begins to produce adenosine triphosphate (ATP), which needs higher glucose than the oxidative phosphorylation procedure. With the depletion of ATP in long-term hypoxia, cell apoptosis and necrosis will happen that eventually fail the graft or scaffold implantation (Pathi et al., 2013).

Since O<sub>2</sub> is essential for cell metabolism and survival, several studies have been conducted with the aim of oxygen delivery to implanted tissues and scaffolds (Ashammakhi et al., 2019a). To this end, oxygen can be provided either directly or indirectly, generating O<sub>2</sub> in an indirect way through chemical reactions, such as loading peroxides within a polymeric substrate (oxygen-generating biomaterials (OGBs) (Gholipourmalekabadi et al., 2016; Kagawa et al., 2015). Among the various oxygen delivery systems, calcium peroxide (CPO) is recognized as a safe, sustainable, and controllable OGB for delivering oxygen (Camci-Unal et al., 2013). CPO generates oxygen in aqueous environments, and calcium hydroxide is produced during the oxygenation as a byproduct (An et al., 2019). Compared with other peroxides (e.g., magnesium peroxide, sodium percarbonate, and hydrogen peroxide), CPO has higher purity and more controllable oxygenation; thus, it has gained lots of attention for OGBs (Agarwal et al., 2021). Since calcium ions are present in this

chemical reaction, it is helpful to use CPO for tissues like bone and heart, where calcium plays a significant role in their function. OGBs are encapsulated mostly in polymeric substrates to reduce the possibility of burst oxygen generation and byproducts release (de Sousa Araújo et al., 2021). Some polymers that have been utilized as polymeric substrates for OGBs are poly(lactide-coglycolide) (PLGA) (Daneshmandi and Laurencin, ), polylactic acid (PLA) (Khorshidi et al., 2021), poly(trimethylene carbonate) (PTMC) (Steg et al., 2017), polycaprolactone (PCL) (Guaccio et al., 2011), poly(N-vinylpyrrolidone) (PVP), elastomeric antioxidant polyurethane (PUAO) (Shiekh et al., 2018), polydimethylsiloxane (PDMS) (Pedraza et al., 2012), polytetrafluoroethylene (PTFE) (Farling et al., 2021) and gelatin methacryloyl (GelMA) (Alemdar et al., 2016). The hydrophobic biopolymers are suggested for OGBs fabrication since this structure could slow down the oxygen generation and delivery and provide an extended supply of O<sub>2</sub>. Most of the used hydrophobic polymers are synthetic ones; thus, it is worth examining the features of OGBs embedded in natural polymers that can be counted as hydrophobic. For instance, we developed a novel OGB made of CPO and silk fibroin through electrospinning, representing the high ranges of oxygen release merely by loading 0.1%, 0.5% and 1% wt of CPO (Aleemardani et al., 2020). Compared with similar studies, the given results were within equal or greater amounts of released oxygen (Khorshidi et al., 2021; Khorshidi and Karkhaneh, 2021; Suvarnapathaki et al., 2021a).

Silk fibroin (SF) has been widely investigated for delivery systems, regenerative medicine, and tissue engineering, owing to its exceptional properties, among other biopolymers (both natural and synthetic) (Farokhi et al., 2018; Watanabe et al., 2021). This natural protein-based polymer has biocompatibility, biodegradability, high oxygen uptake, low immunogenicity, amphiphilic structure, and robust mechanical properties (Sammi et al., 2021). SF entails dominant hydrophobic segments in its structure, making it a proper candidate for achieving controllable and sustainable

release (Pritchard and Kaplan, 2011). SF has high processability and can be processed in various forms like fibers and hydrogels, and each type has its particular characteristics (Reimers et al., 2015). Hydrogels are counted as the forefront type of material for biomedical applications. Hydrogels are three-dimensional (3D) networks containing physical and chemical crosslinked polymeric structures that show a high ability to absorb large amounts of water. Hydrogels have extensive use in biomedicine, particularly tissue engineering, because of their mechanical similarity to the native extracellular matrix (ECM) and the capacity for loading drugs, bioactive molecules, and cell encapsulation (Aleemardani et al., 2021a; Tran et al., 2020).

Quercetin (Q), a plant flavonol from the flavonoid polyphenol group, is found in many fruits, vegetables, leaves, and seeds. In recent years, Q has become the focus of medical researchers' attention due to its multiple pharmacological effects. In addition to antitumor, antiviral, antibacterial, anti-aggregatory, and significant heart-related benefits, many studies have shown that Q is a potent non-enzymatic antioxidant appropriate for scavenging oxygen free radicals; also, it is mainly used as an antioxidant reference due to its high activity (Cirillo and Iemma, 2012; Gori et al., 2021). However, despite the vast potencies of Q, its applications have faced some limitations owing to its low water solubility (Sheng et al., 2020). So far, some studies contain the Q and SF combination (Lozano-Pérez et al., 2017; Song et al., 2018), but this study evaluates the effect of Q on SF gelation for the first time. Further, in this study, we introduce Q as a non-enzymatic antioxidant that is highly stable and can scavenge free radicals.

This study aims to develop composite scaffolds for the controlled release of oxygen based on SF. Given the benefits of SF, particularly having high biocompatibility, oxygen permeability, and amphiphilic structure, which has dominant hydrophobic segments, this natural polymer can be a suitable option for incorporating OGBs (e.g., CPO) as well as poor water-soluble drugs or

biomolecules (e.g., Q). In order to achieve controlled oxygen release, the SF-CPO composites were first produced by electrospinning (Aleemardani et al., 2020); among them, E(SF-1CPO) containing 1% wt CPO was embedded between the two layers of physical SF hydrogel (hydrogel-fiber-hydrogel, composite scaffold). Further, to reduce or eliminate possible oxygen free radicals (ROS), Q (present in the SF hydrogels) was used. Further, to reduce or eliminate possible oxygen free radicals (ROS), Q (present in the SF hydrogels) was used. Enzymatic antioxidants like catalase have been widely used in OGB studies to inactivate potential free radicals, but the main challenge of this method is maintaining enzymatic stability. However, the present study used a non-enzymatic antioxidant (Q), which is more stable than an enzymatic antioxidant (Agarwal et al., 2021; Cirillo and Iemma, 2012; Wang et al., 2016). Also, Q can scavenge potential free radicals as well as have other biomedical properties. Previously, we studied the fabrication and evaluation of electrospun SF-CPO patches as unique OGBs (Aleemardani et al., 2020). In the present study, we aim to investigate the fabrication and performance of composite scaffolds as OGBs for tissue engineering applications proposed for bone, which contain three layers: (1) SF hydrogel, (2) electrospun fibres and (3) SF hydrogel. SF fibers supply oxygen delivery and enhance mechanical strength, while the other two layers, SF hydrogels, containing Q provide the sustained release, antioxidant and antibacterial properties.

## **2. Materials and Methods**

### **2.1. Materials**

*Bombyx mori* (*B. mori*) silkworm cocoons were obtained from the University of Guilan (Rasht, Iran). Lithium bromide (LiBr), 12 KDa cut-off dialysis membrane, Alizarin Red S, glutaraldehyde, calcium peroxide powder (CPO), Quercetin (Q), and 2,2-diphenyl-1-

picrylhydrazyl (DPPH) were purchased from Sigma-Aldrich. Sodium carbonate, hexafluoro-2-propanol (HFIP), methanol, ethanol, acetic acid, and dimethyl sulfoxide (DMSO) were obtained from Merck. The utilized phosphate buffer saline (PBS) in all tests was obtained from Gibco.

## **2.2. Preparation of Silk Fibroin Solution**

SF solution was prepared following the procedure published previously by Aleemardani et al. (Aleemardani et al., 2020). First, cut *B. mori* cocoons were degummed to eliminate the sericin through boiling in the alkaline water bath (0.02 M Na<sub>2</sub>CO<sub>3</sub>) for about 40 min. Degummed SF was then rinsed with distilled water three times and dried overnight at room temperature. The degummed silk fibers were dissolved in 9.3M LiBr at 60 °C for 4 h; subsequently, the solution was dialyzed against distilled water for 3 days in a dialysis membrane. Later, the SF solution was centrifuged (Sigma 4-15c, Germany) for 30 min at 4000 rpm to remove impurities. From the changes in wet and dry weights of SF, the protein concentration was measured, and concentration was adjusted with distilled water to 3% w/v.

## **2.3. Physical Silk Fibroin Hydrogel Formation**

Ultrasonication was used to form physical SF hydrogels. The SF solution was subjected to probe ultrasonication (Hielscher, UP400S, Germany), at 40% amplitude for 30 sec (Fernández-García et al., 2016), and gelation was completed at 37 °C. The ultrasonication was done with ice at 0 °C to control the temperature. The gelation time of the samples was calculated from when the sample was at 37 °C (Seib et al., 2013). It was considered that the viscosity of the sample in the container (mold) entailing hydrogel was increased to such an extent that the sample did not flow after the container was inverted (Sarker et al., 2014).

## **2.4. Physical Silk Fibroin-Quercetin Hydrogel Formation**

A Q concentration of 50-500  $\mu\text{M}$  was used, which was previously shown to have significant antioxidant activity and no cytotoxicity (Hatahet et al., 2016). The viability assay (at 65, 100, 200, and 400  $\mu\text{M}$  Q in DMSO solvent) was performed on MG-63 cells to determine the appropriate drug amount. Subsequently, based on the viability assay results, the desired concentration (400  $\mu\text{M}$ ) was selected and loaded into the SF solution. Then SF hydrogels entailing Q were fabricated by the physical method described in Section 2.3.

## **2.5. Fabrication of Composite Scaffolds**

The composite scaffold is composed of three layers (Figure 1): (1) physical SF hydrogel (with or without Q), (2) the SF-CPO electrospun patches (containing 1% wt CPO) (Aleemardani et al., 2020), and (3) physical SF hydrogel (with or without Q). The composites were stored at -20  $^{\circ}\text{C}$  for 24 h and lyophilized (Christ-GAMMA2-16LSC) at -80  $^{\circ}\text{C}$  for 24 h.

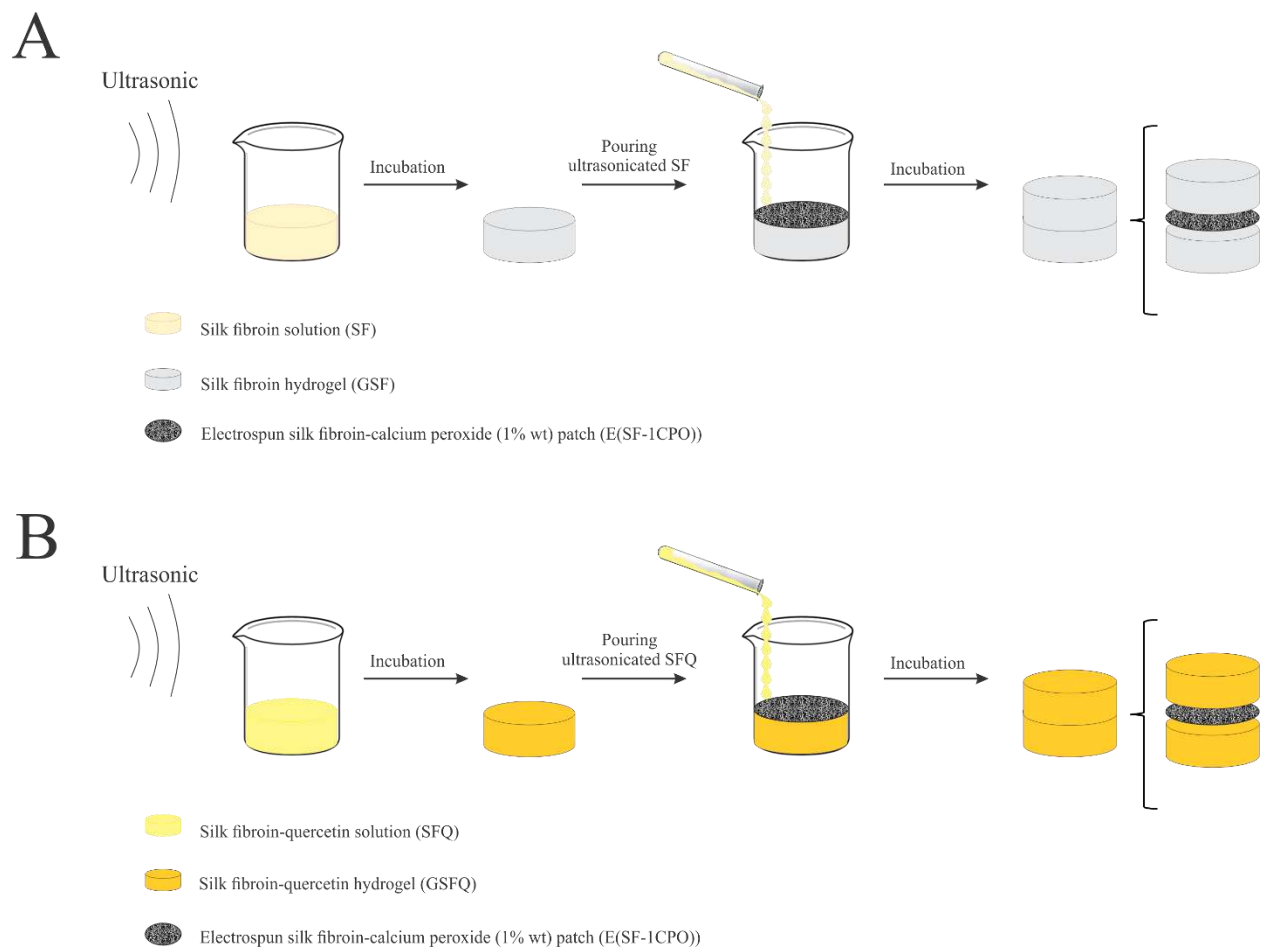


**Figure 1.** The schematic of composite scaffolds fabrication: (A) consisting of physical silk fibroin hydrogel (GSF) and electrospun silk fibroin-calcium peroxide (1% wt) patch (E-(SF-1CPO)) or labeled as GSF-E(SF-1CPO) and (B) consisting of physical silk fibroin-queracetin hydrogel (GSFQ) and electrospun silk fibroin-calcium peroxide (1% wt) patch (E-(SF-1CPO)) or labeled as GSFQ-E(SF-1CPO).

## 2.6. Characterization

### 2.6.1. Monitoring the Gelation Process

Solutions (SF and SFQ) were incubated at 37 °C after sonication, and the sol-gel transition was monitored visually, as previously reported by Wang et al. (Matsumoto et al., 2006). Turbidity changes were measured with a UV/Vis spectrophotometer (ELX808, BioTeK, USA) to monitor the gelation process at 37 °C at 550 nm.

### **2.6.2. Scanning Electron Microscopy (SEM)**

Images were captured by scanning electron microscope (SEM) (Seron Technologies, AIS2100, South Korea) to observe the structure, morphology, and porosity. In order to intensify signal quality, samples were sputter-coated (Emitech, SC7620-1KV Dc) with gold at 20 kV voltage before imaging.

### **2.6.3. Fourier Transform Infrared Spectroscopy (FTIR)**

Freeze-dried hydrogels were ground to powder, then mixed with KBr salt, and pressed into a tablet. Subsequently, the tablets were mounted in an infrared spectrometer (iS10, Thermofisher, Germany). The FTIR spectrum was obtained from 400-4000  $\text{cm}^{-1}$  wavenumber at transmittance mode with a resolution of 4  $\text{cm}^{-1}$  and 64 scans per sample.

### **2.6.4. Pore Size and Porosity Analysis**

The pore size and surface porosity of the hydrogel were calculated based on the SEM images by ImageJ software (Loh and Choong, 2013). To measure the porosity of hydrogels, circular porosity was selected, and 5 diameters (5 diameters per image; 5 images per sample type) were measured through ImageJ (ver.1.5.2) for each. The diameters were expressed as the mean $\pm$ standard deviation (SD).

The bulk porosity of the scaffolds (hydrogels and composites with 1×1 cm<sup>2</sup>: diameter × height) was measured using water absorption according to Eq. 1 (Loh and Choong, 2013). For this purpose, freeze-dried samples were first weighed ( $W_{dry}$ ) and placed in water until complete adsorption, achieving an equilibrium point. The samples were then removed from the water and weighed again ( $W_{wet}$ ).

$$\text{Porosity (\%)} = [(W_{wet} - W_{dry}) / W_{wet}] \times 100 \quad (1)$$

### 2.6.5. Swelling Properties

Firstly, the weight of dried scaffolds (hydrogels and composites) was measured ( $W_{dry1}$ ). Secondly, the samples were immersed in phosphate buffer saline (PBS) at 37 °C and sampled at defined time intervals ( $W_{hyde}$ ) until reaching a constant weight ( $W_{wet}$ ). Finally, after the complete drying, the weight of scaffolds was again measured ( $W_{dry2}$ ). The water uptake ratio and swelling percentages were calculated as follows (Eq. 2 and Eq. 3) (Khorasani et al., 2018):

$$\text{Swelling (\%)} = [(W_{wet} - W_{dry2}) / W_{dry2}] \times 100 \quad (2)$$

$$\text{Water uptake rate} = [(W_{wet} - W_{dry1}) / W_{dry1}] \quad (3)$$

### 2.6.6. Biodegradation

To investigate the degradation process of the samples, freeze-dried scaffolds were prepared at 1 cm (diameter) × 1 cm (height). The initial weight of dry specimens ( $W_{dry1}$ ) was measured, and samples were placed in PBS (pH = 7.4 at 37 °C) for specific time intervals. After each interval, the samples were thoroughly dried and weighed ( $W_{dry2}$ ), and weight loss with the help of Eq. 4 was calculated for a month.

$$\text{Biodegradation (\%)} = [(W_{dry1} - W_{dry2}) / W_{dry1}] \times 100 \quad (4)$$

### **2.6.7. Mechanical Properties**

The compressive properties of the scaffolds were investigated through a universal mechanical testing machine (Instron, 5565, United States) at room temperature. The specimens were cylindrical, with a diameter of 1 cm and a height of 1 cm. For the tests, a compression rate of 1 mm/min was used to reach 40% of their initial size. 3 sets of parallel samples were measured. The test was conducted to stimulate the physiological environment after soaking the scaffolds in PBS at 37 °C for 24 h. In addition, to analyze the reversibility, the load was removed at the same rate to obtain the specimens' hysteresis diagrams. The reversibility was calculated from the height before loading ( $h_1$ ) and after loading ( $h_2$ ) (Eq. 5) (Harrass et al., 2013):

$$\text{Reversibility (\%)} = [(h_2-h_1)/h_1] \times 100 \quad (5)$$

### **2.6.8. Oxygen Release Study**

Oxygen release was measured using a blood gas analyzer (MEDICA EasyStat, USA). The scaffolds ( $1 \times 1 \text{ cm}^2$ : diameter  $\times$  height) were transferred into a 15 ml cylindrical vial containing 5 ml of phosphate buffer (PBS). Samples were incubated at 37 °C under normal conditions (normoxia). At the time of oxygen measurement, 1 ml of the solution was removed using a syringe, the dissolved oxygen was determined, and then 1 ml of fresh PBS was added to the vial. The oxygen release from three scaffolds was analyzed to determine the mean and standard deviation for each sample.

### **2.6.9. Antioxidant Activity Analysis**

To investigate the antioxidant activity of scaffolds, the ability and efficacy to inhibit the activation of free radicals were determined by 2,2-diphenyl-1-picrylhydrazyl (DPPH) assay according to the method reported by Selvaraj et al. (Selvaraj and Fathima, 2017). 5 mg of samples

were added in 3 mL of 100  $\mu$ M DPPH solution in methanol and then incubated in the dark for 30 minutes. Subsequently, the wavelength scanning was performed by a UV-Vis spectrophotometer (AnalytikJena, Specord 210, Jena, Germany). DPPH degradation was measured through the following formula (Eq. 6).

$$\text{Percentage of DPPH scavenging (\%)} = [(A_B - A_S)/A_B] \times 100 \quad (6)$$

Where  $A_B$  and  $A_S$  are the absorbance of the blank and the sample at 517 nm, respectively.

For the time-dependent assay, 5 mg of the GSFQ-E(SF-1CPO) was placed in 1 ml of phosphate buffer (PBS) for different times. Then, the suspension was incubated in 1 ml of 100  $\mu$ M DPPH solution for 30 min. Afterward, the absorbance was measured at 517 nm (Selvaraj and Fathima, 2017).

#### **2.6.10. Antibacterial Activity**

Methicillin-resistant *Staphylococcus aureus* (MRSA) has been a clinically dangerous pathogen in orthopedics, and it was chosen because the fabricated scaffolds are considered for bone tissue engineering applications. For this test, the Kirby-Bauer technique was followed. Firstly, the blank discs got smeared with Q powder (control), hydrogel (GSFQ), and composite (GSFQ-E(SF-1CPO)) in powder form with the weight of 0.01 g and subsequently placed on a nutrient agar plate with  $1 \times 10^7$  CFU of MRSA. After being incubated overnight (at 37 °C), the inhibition zone was measured. Noteworthy, the specimens became wet with Dulbecco's phosphate-buffered saline (DPBS, Gibco) because the antibacterial activity was negligible in the dry state.

#### **2.6.11. Cellular Assays**

#### **2.6.11.1. Evaluation of Cell Viability in the Vicinity of Quercetin**

Approximately 4000 MG-63 cells were cultured in each well (in a 96-well plate), and desired concentrations of Q (65, 100, 200, and 400  $\mu\text{M}$ ) were added to the culture medium and incubated for 24 h. Then, the culture medium was removed, 3-(4,5-dimethylthiazol-2-yl)-2,5-diphenyltetrazolium bromide (MTT, Roth) (0.5 mg/ml) was added, and the cells were incubated for 4 h. After removing the medium, DMSO was substituted, and the absorbance of the samples was read at 570 nm by ELISA (ELx808, USA). Each sample was replicated 5 times, and the cell viability bar chart was plotted.

#### **2.6.11.2. Evaluation of Cell Viability of Scaffolds**

To evaluate the effect of oxygen delivery and quercetin on cell viability and proliferation, the MTT assay was carried out (ISO 10993). The human MG-63 osteoblast cells were seeded on the scaffolds (hydrogels and composites) with a  $10^4$  cell density and cultured in an expansion medium composed of a 1:1 mixture of Dulbecco's modified Eagle medium and Ham's F-12 medium (DMEM/F-12) supplemented with 10% (v/v) Fetal Bovine Serum (FBS) and 1% antibiotic penicillin/streptomycin (Gibco, USA). Following the incubation in two conditions (at 37 °C in 5%  $\text{CO}_2$  (normoxia) and at 37 °C in 5%  $\text{O}_2$  and 5%  $\text{CO}_2$  (hypoxia)) for various intervals (1, 3, and 6 days), the medium was removed. Subsequently, the MTT solution (0.5 mg/ml) was poured into each well, followed by 4 h incubation. Then, the MTT was substituted by dimethyl sulfoxide (DMSO, Sigma-Aldrich). Finally, the absorbance was measured at 570 nm with an ELISA reader (ELx808, US). The replication for each scaffold was five times.

#### **2.6.12. Statistical analysis**

The results are presented as mean±standard deviation (SD). Statistical analyses were performed with IBM SPSS Statistical 23 software. Significant differences (p-value) were identified using one-way ANOVA and Tukey's post hoc analysis. The replication for each scaffold was three times for each test; otherwise, it has been mentioned in the materials and methods section.

### **3. Results and Discussion**

#### **3.1. Monitoring the Gelation Process**

The sol-gel transition occurs during gelation when random coil structures of the SF are transformed into the  $\beta$ -sheet structures, and the percentage of transition affects the hydrogel properties. Upon gelation, opaque white color is visible due to the heterogeneous microstructure of the SF gel that causes light scattering in the visible light range. Therefore, to track the gelation, optical density (OD) changes should be evaluated at 550 nm (Farokhi et al., 2021). There are some studies with SF and Q combinations in the forms of sponges or nanoparticles (Diez-Echave et al., 2021); however, to the best of our knowledge, this is the first study investigating the effects of Q on SF gelation, so it is significant to understand OD changes. To determine the gelation time and opacity changes, OD was measured at 550 nm over 11 days; the results of OD and visual observations are reported in Figure 2. The OD alters with time for solutions: at first faces an upward trend and then stabilizes at the values where all solutions have gelled (Figure 2A). Alterations of OD indicate changes in the SF secondary structure ( $\beta$ -sheets) during the gelation transition (Farokhi et al., 2021). As shown in Figure 2, the presence of Q led to a decrease in gelation time. On day 3, SFQ was more opaque than SF, which can be due to the hydroxyl groups present in Q and the crosslinking with SF molecules. Also, the GSFQ specimens are yellowish

because of loaded Q, and SFQ samples had higher OD values from day 0. Therefore, it is possible that Q has a high absorbance (OD) and results in greater OD over time; however, the degree and percentage of gelation could be lower.

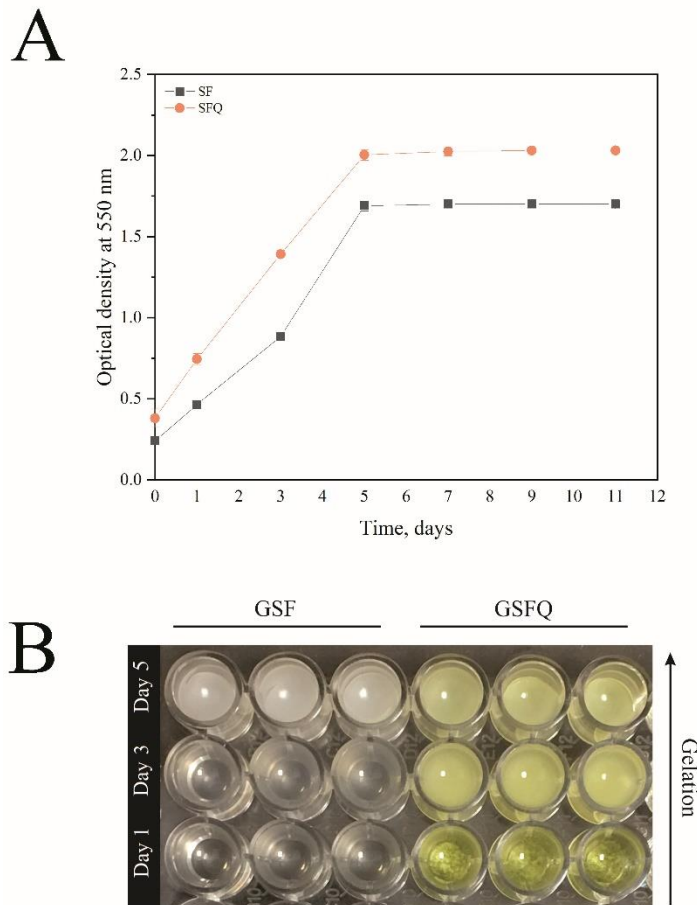


**Figure 2.** (A) Optical density changes at 550 nm of the solutions (SF and SFQ) in a 96-well plate (200  $\mu$ L in each well) prepared at 37  $^{\circ}$ C at various time intervals, and (B) image of SF gels (GSF and GSFQ) at day 1, 3, and 5 prepared at 37  $^{\circ}$ C in a 96-well plate (200  $\mu$ L in each well) (n = 3).

### 3.2. Scanning Electron Microscopy (SEM)

The images were taken from the cross-sections of the specimens with two scales to examine the morphology and internal microarchitectures of the porous scaffolds. SEM images of GSF, GSFQ, GSFQ-E(SF-1CPO) and E(SF-1CPO) are given in Figure 3. The GSF showed porous structures with a diameter of  $102.22 \pm 12.12 \mu\text{m}$  (Figure 3A). Through ultrasonication, polymer chains have been converted from random arrangement ( $\alpha$ -helix) to regular structure ( $\beta$ -sheets), and during this process, interconnected porosity has been created. Guziewicz et al. found that a higher amplitude and duration of ultrasonication result in more top  $\beta$ -sheets formation; therefore, the size of the porosity of SF hydrogel decreases, and a denser structure is formed (Guziewicz et al., 2011). The sonication parameters in our study were chosen based on the required porosity size, and the obtained size is suitable for osteoblasts proliferation and migration. The SEM images of the GSFQ depict a significantly larger pore size ( $191.08 \pm 9.81 \mu\text{m}$ ) than the GSF ( $p < 0.01$ ) (Figure 3B). To the best of our knowledge, there is no previous report of SF hydrogels that contain Q (both physically and chemically). However, in the present study, the production of SF hydrogel with Q was considered. It should be noted that the presence of Q played a role in the formation of hydrogels, and it had a noticeable impact on the gelation time and porosity. It can be hypothesized that the presence of Q led to lower gelation and resulted in larger pores. It is also possible that an increase in porosity as a function of loading Q into the scaffolds was due to the formation of ice crystals after their removal from Q-DMSO solution during freeze-drying (Song et al., 2018). Figure 3C shows the SEM images of the GSFQ-E(SF-1CPO) composite scaffold. According to the images, the morphology of the fibers is fully preserved during gelation and freeze-drying, and there is a three-layer composite structure (gel-fiber-gel). By combining porous hydrogel and electrospun fibers, composite scaffolds can be developed to mimic the natural structure of tissues or organs like bone by providing better cellular penetration (Loh and Choong, 2013).

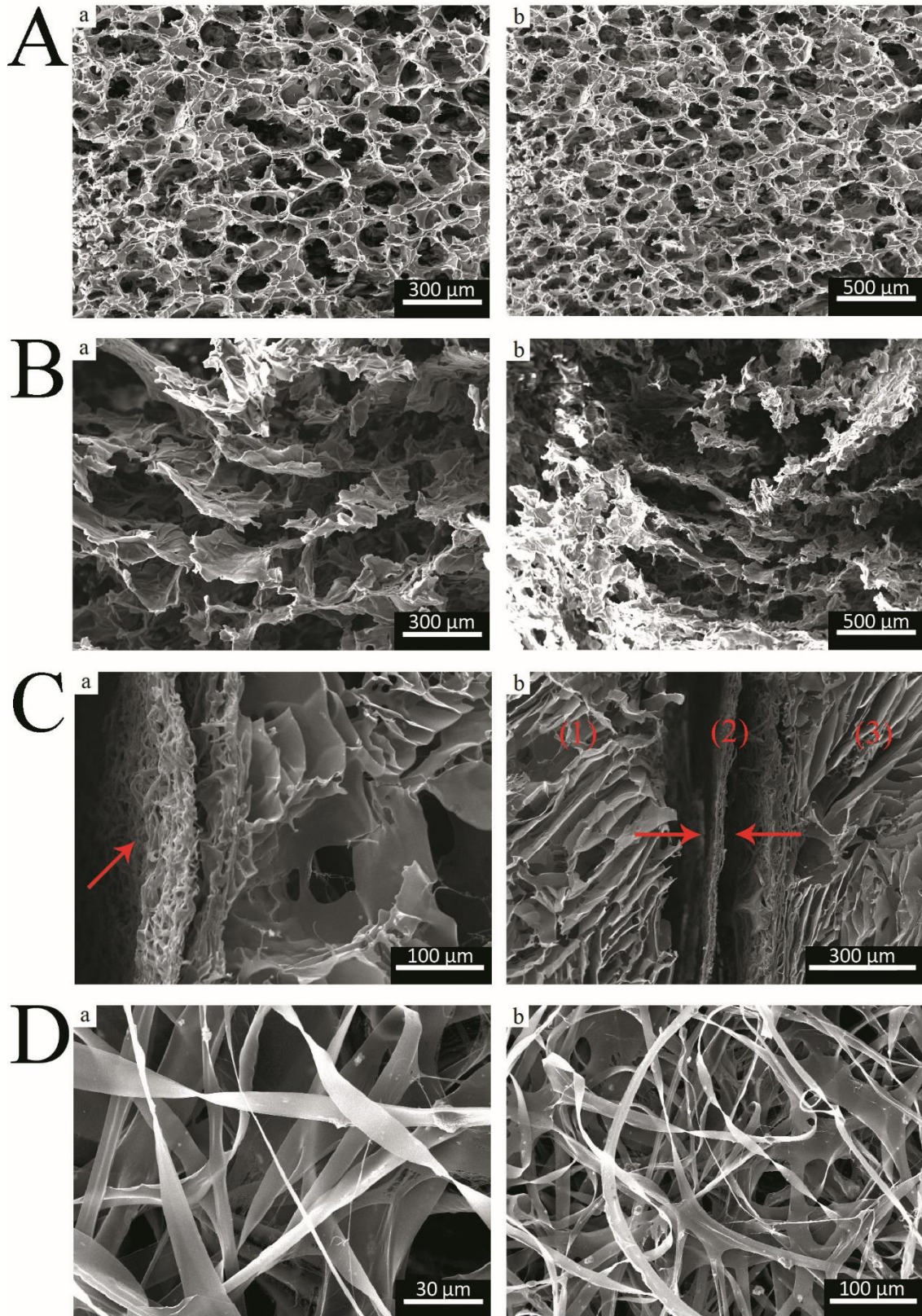


**Figure 3.** SEM images of (A) GSF hydrogels, (B) GSFQ hydrogels (with scales of a: 300 and b:

500  $\mu\text{m}$ ), (C) GSFQ-E(SF-1CPO) composite scaffold, having three layers: (1), (3) GSFQ hydrogel and (2) E(SF-1CPO) patch (with scales of a: 100 and b: 300  $\mu\text{m}$ ) and (D) E(SF-1CPO) fibers (with scales of a: 30 and b: 100  $\mu\text{m}$ ).

### 3.3. Fourier Transform Infrared Spectroscopy (FTIR)

Figure 4A shows the FTIR spectra of the GSF, GSFQ, and Q; the results of FTIR of SF extraction and electrospun patch, E(SF-1CPO), are reported in our previously published work (Aleemardani et al., 2020). The FTIR spectra of GSF show sharp peaks at 1624  $\text{cm}^{-1}$  (amide I), 1527  $\text{cm}^{-1}$  (amide II), and 1232  $\text{cm}^{-1}$  (amide III). The mentioned peaks not only reveal the presence of SF but also display an increase in the crystalline structure of  $\beta$ -sheets (due to the sonication and gelation process) (Li et al., 2020). Besides, in GSFQ, the peaks related to SF (amide I, amide II, and amide III) are visible. Notably, amide II (1521  $\text{cm}^{-1}$ ) had a more significant displacement towards the  $\beta$ -sheets. The presence of Q in GSFQ was also investigated, and it was observed that SF index peaks (amides) largely overlapped with Q peaks (Song et al., 2018; Yadav et al., 2020). However, in the range of wavenumbers 500-1000  $\text{cm}^{-1}$  (precisely at 842, 823, 795, 721, 638 and 606  $\text{cm}^{-1}$ ), Q peaks are apparent in the FTIR spectra of GSFQ (Catauro et al., 2015; Jang et al., 2020; Li et al., 2020; Lozano-Pérez et al., 2017; Milanezi et al., 2019). Table 1 lists the various FTIR spectra peaks related to the specimens (GSF, GSFQ, and Q) used in the study.

**Table 1.** Index peaks of biomaterials used in presented research (Catauro et al., 2015; Jang et al., 2020; Li et al., 2020; Lozano-Pérez et al., 2017; Milanezi et al., 2019).

<b>Biomaterial</b>	<b>Reported wavelength (cm<sup>-1</sup>)</b>	<b>Wavelength (cm<sup>-1</sup>)</b>	<b>Bond</b>
SF (founded in GSF and <b>GSFQ</b> )	3000-3800	3287 and 3285	-OH stretching
	1600-1700 (Amide I)	1624	C=O stretching
	1500-1600 (Amide II)	1527 and <b>1521</b>	N-H bending
	1200-1300 (Amide III)	1232 and <b>1231</b>	C-H stretching
Q (founded in Q and <b>GSFQ</b> )	3300-3700	3404, 3314	O-H stretching
	1670	1664	C=O absorption
	1612	1611	C-C stretching
	1456, 1383, 866	1450, 1381, 864	C-H bending
	1272	1261	C-O stretching in the ring structure
	1070, 1150	1169, 1092	C-O stretching
	600-1000	603, 638, 721, 794, 824, 842, 846 and 932 and <b>606, 638, 721, 795, 823 and 842</b>	Angular deformation of C=CH of the aromatic compounds

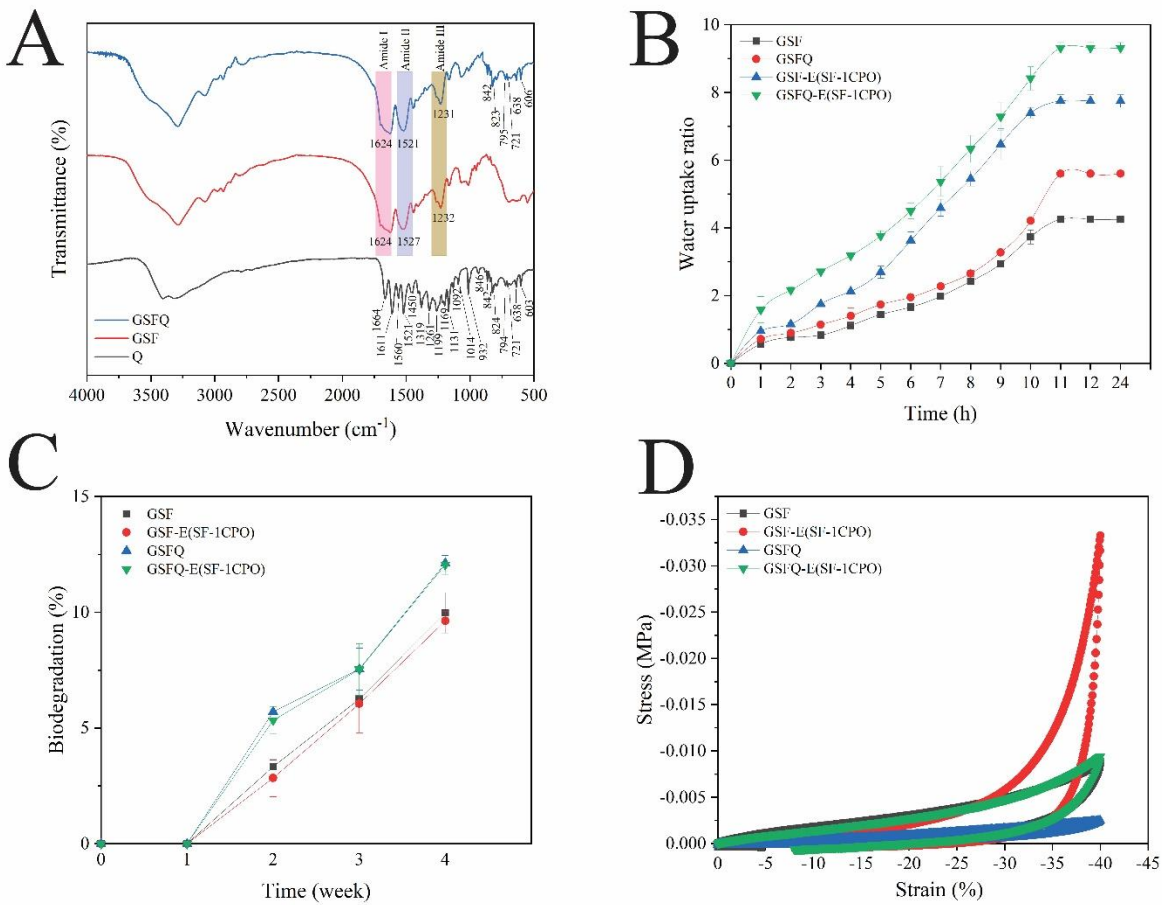


**Figure 4.** (A) FTIR spectra of Q powder, GSF and GSFQ hydrogels. (B) The diagrams of water uptake ratio, (C) biodegradation and (D) stress-strain diagram of hydrogels (GSF and GSFQ) and composites (GSF-E(SF-1CPO) and GSFQ-E(SF-1CPO)).

### 3.4. Pore size and Porosity Analysis

The surface and bulk porosity of the hydrogels and composite scaffolds are reported in Table 2. There was no significant difference between the surface porosity of GSF and GSFQ. The bulk porosity of all specimens was above 80%, which indicates a highly porous structure, yet their differences were insignificant. As expected, the porosity (%) in composite scaffolds was enhanced due to the presence of the fibers. Based on the obtained results, the scaffolds are sufficiently porous for adhesion and cell penetration (Nejati et al., 2020; Xu et al., 2016); to exemplify, Karageorgiou

et al. indicated that suitable porosity (i.e., 40-90%) in different biomaterials could increase osteoblast proliferation, bone formation, and implant adhesion (Karageorgiou and Kaplan, 2005).

**Table 2.** Porosity (both surface and bulk) of hydrogels (GSF and GSFQ) and composites (GSF-E(SF-1CPO) and GSFQ-E(SF-1CPO)) (\*,  $\Delta$  and  $\diamond$ :  $p < 0.05$ ).

Sample	Surface porosity (%)	Bulk porosity (%)
GSF	71.33 $\pm$ 0.69	80.95 $\pm$ 0.27 $^{\Delta,*}$
GSFQ	69.35 $\pm$ 1.11	84.85 $\pm$ 0.17 $^{\diamond}$
GSF-E(SF-1CPO)	-	88.56 $\pm$ 0.23 $^{\Delta}$
GSFQ-E(SF-1CPO)	-	90.38 $\pm$ 1.17 $^{*,\diamond}$

### 3.5. Water Uptake

According to Figure 4B, which illustrates the water uptake ratio, it can be stated that the rate and profile of water uptake of GSF and GSFQ were very close to each other. However, the GSFQ had higher water absorption due to its larger pores. The water uptake ratio of hydrogels (GSF and GSFQ) was about 4-5, consistent with other SF hydrogels (Guziewicz et al., 2011). Adding fibers to the GSF-E(SF-1CPO) and GSFQ-E(SF-1CPO) has also helped increase water uptake because the fibers absorb more water due to their high porosity (Xu et al., 2016). All specimens reached their final water uptake before 12 h.

The obtained swelling percentages of GSF and GSFQ were 541.27 $\pm$ 17.11% and 625.87 $\pm$ 12.9%, respectively (similar to the result of the water uptake ratio), and the GSFQ had a higher swelling ( $p < 0.01$ ). The significant increment in water uptake in the samples is critical for all of the hydrogels used in tissue engineering, owing to providing an aqueous environment for

cells, proteins, and growth factors. These hydrogels with high swelling percentages allow the penetration of materials such as oxygen, water-soluble metabolites, and nutrients (Bai et al., 2016).

### **3.6. Biodegradation**

The degradation behavior of the samples in PBS was measured by the weighing method and is shown in Figure 4C. All the scaffolds (hydrogels and composites) were stable in PBS throughout the entire incubation period. The in vitro degradation of GSFQ and GSFQ-E(SF-1CPO) after 1 month was higher than other samples, which is related to larger porosity, which results in accelerated degradation rates.

### **3.7. Mechanical Properties**

Figure 4D depicts the elastic behavior of the specimens with the hysteresis diagram and the elastic region diagram to calculate Young's modulus. The addition of Q reduced Young's modulus due to increased porosity. However, the addition of fibers can compensate for this reduction to some extent (Choi et al., 2020). Composite scaffolds (GSF-E(SF-1CPO) and GSFQ-E(SF-1CPO)) had a higher Young's modulus and compressive strength ( $p < 0.01$ ) (Table 3). It should be noted that the larger diameter of fibers results in higher mechanical properties of the composite scaffold (Yodmuang et al., 2015); in the present study, the fiber diameter was roughly 13  $\mu\text{m}$  which led to doubling the mechanical strength. The Young's modulus and the compressive strength obtained, as given in Table 3, are consistent with other studies (Samal et al., 2014; Song et al., 2018). Scaffolds containing Q had larger pores and lower mechanical strength. As mentioned in the section on porosity analysis, it can be due to the presence of Q solution (in DMSO solvent);

that is why it is possible to form larger ice crystals. Larger pores reduce the mechanical properties that can be seen in the obtained results (Table 3) (Song et al., 2018).

The compressive strength of the specimens was 0.23-0.6 MPa. Studies have shown that dense and spongy bone tissue's compressive strength is 100-230 MPa, and 2-12 MPa, respectively. Therefore, designed scaffolds can be suitable for different clinical procedures due to the lower compressive strength, depending on the location and type of the defect (Mohamed and Shamaz, 2015); for instance, they can be used for cranial bones (Suvarnapathaki et al., 2021b). Moreover, the reversibility behavior of the samples during the process was observed. The scaffolds were pressurized to 40% of their initial length and returned to their initial state after removing the pressure. The reversibility is presented quantitatively by measuring the changes in the length (before and after applying the pressure) in Table 3.

**Table 3.** Young's modulus, compressive strength and reversibility results of hydrogels (GSF and GSFQ) and composites (GSF-E(SF-1CPO) and GSFQ-E(SF-1CPO)) ( $\Delta$ :  $p < 0.01$  and  $^{**}$ :  $p < 0.05$ ).

Sample	Young modulus (KPa)	Compressive strength (MPa)	Reversibility (%)
GSF	8.5±0.2 $\Delta$	0.43±0.03 $^*$	94.17±3.24
GSFQ	4.27±0.15 $\Delta$	0.23±0.02 $^{**}$	95.09±3.03
GSF-E(SF-1CPO)	15.7±0.1 $\Delta$	0.60±0.02 $^*$	93.85±4.02
GSFQ-E(SF-1CPO)	8.27±0.25 $\Delta$	0.38±0.03 $^{**}$	94.66±4.44

### 3.8. Oxygen Release Study

To determine the duration of oxygen release by composites (GSF-E(SF-1CPO) and GSFQ-E(SF-1CPO)), the concentration of dissolved oxygen was measured over 12 days. The dissolved oxygen amounts in the presence of GSF were also assessed as a control sample. Figure 5A shows the release profile of composite scaffolds and control. The oxygen concentration is higher for composite scaffolds than for electrospun fiber scaffolds (Aleemardani et al., 2020), which can be due to the presence of larger pores in hydrogels. Larger pores of hydrogels trap more air, and in the presence of an aqueous environment, oxygen dissolution over time (the air trapped in these pores) increases oxygen concentration. In composites, the maximum oxygen release occurred on day 6. Thus, the presence of a hydrogel structure leads to a delay in oxygen release; for electrospun fibers, maximum oxygen release was on day 3 (Aleemardani et al., 2020). The GSFQ-E(SF-1CPO) oxygen release profile was higher than the GSF-E(SF-1CPO); this could be due to the presence of the antioxidant Q, which makes the release of oxygen more stable and promotes the hydrolysis reaction (the reaction of CPO and water to generate oxygen). In a similar study, Abdi et al. depicted that catalase, an enzymatic antioxidant, leads to the sustainable release of oxygen and reduces free radicals, ultimately increasing cell viability (Abdi et al., 2011). When the hydrolysis is complete, free radicals will not be produced, so it can be adduced that antioxidants stabilize oxygen release. The amount of generated oxygen from composite scaffolds is within the range that is appropriate for beta cells (0.08-155 mmHg) (Coronel et al., 2019), hepatocytes (~30-65 mmHg) (Farzaneh et al., 2020; Kang et al., 2020), osteoblasts (~10-35 mmHg) (Khorshidi et al., 2019; Khorshidi and Karkhaneh, 2021; Touri et al., 2019), cardiac muscle cells (~20-50 mmHg) (Wang et al., 2021), and epithelial cells (~8-13 mmHg) (Lv et al., 2016). Previous studies reported significant bone regeneration improvement with two weeks of oxygen released from the scaffolds (Suvarnapathaki et al., 2021b; Touri et al., 2020). Therefore, a suggested application can be for bone tissue

engineering because of the suitable mechanical strength and oxygen release of scaffolds. Furthermore, the pH alteration was measured during the release, ranging from 7.30-7.57 (Figure 5B). Due to the calcium peroxide and water reaction, changes in pH had a similar trend to the oxygen release profile regardless of some points. The highest pH was measured on the sixth day (7.57 for the GSF-E (SF-1CPO)); the pH profiles of both composites were very close.

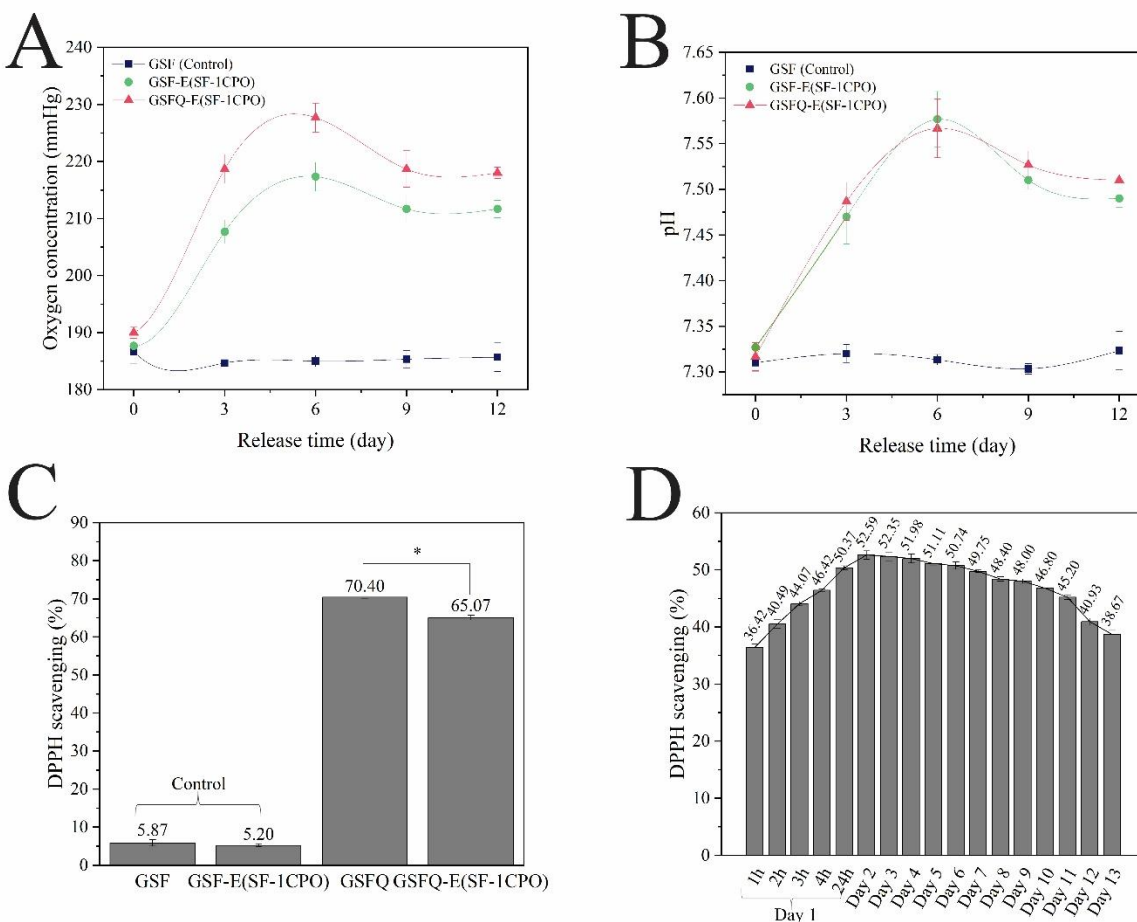


**Figure 5.** (A) Oxygen profile release over 12 days and (B) pH changes over 12 days. The percentages of DPPH scavenging for (C) hydrogels (GSF and GSFQ) and composites (GSF-E(SF-1CPO) and GSFQ-E(SF-1CPO)) (\*:  $p < 0.05$ ) and (D) for GSFQ-E(SF-1CPO) within 13 days.

### 3.9. Antioxidant Activity Analysis

Various studies have shown that the presence of additional free radicals (especially ROS) can upset the balance between oxidative-antioxidant states of cells (Alizadeh and Ebrahimzadeh, 2021). Therefore, it is expected that the antioxidants will minimize the adverse effects of the presence of additional free radicals at the oxygen release site (Lobo et al., 2010). Hence, the presence of antioxidants stabilizes oxygen release and improves cell viability (Abdi et al., 2011). So far, using catalase, an enzymatic antioxidant within the cells, for OGBs is widely accepted, although its main problem is instability over time.

To this aim, Q, a non-enzymatic antioxidant, has been used for the first time for a OGB in order to inactivate the possible free radicals during oxygenation. This non-enzymatic antioxidant is quite stable and multifunctional; therefore, Q not only can scavenge the free radicals like ROS but also can bring other features for OGBs like antibacterial properties (Amer et al., 2021; Sayyad et al., 2021). To investigate the effect of Q on free radicals, it is necessary to evaluate the antioxidant properties of specimens. For this purpose, a DPPH assay was utilized (Caddeo et al., 2019). The percentages of DPPH scavenging are given in Figure 5C. GSF and GSF-E(SF-1CPO) antioxidant activity (control samples) were  $5.87\pm 0.83\%$  and  $5.20\pm 0.4\%$ , respectively. SF contains the tyrosine and tryptophan amino acids in the phenolic side chains, which may be the reason for the antioxidant activity of controls (Selvaraj and Fathima, 2017). However, the depicted antioxidant activity of GSFQ ( $70.40\pm 0.4\%$ ) and GSFQ-E(SF-1CPO) ( $65.07\pm 0.61\%$ ) was remarkably high. Lower GSFQ-E(SF-1CPO) antioxidant activity (compared to GSFQ) might be due to the presence of a breathable electrospun patch (E(SF-1CPO)). The significant inactivation of DPPH in the presence of Q can be attributed to the transfer of electrons from Q loaded in the scaffold structure to DPPH radicals (Caddeo et al., 2019). Besides, for time-dependent measurements, the GSFQ-E(SF-1CPO) antioxidant activity was assessed at different time intervals

for 13 days (Figure 5D). Due to the loading of Q in SF hydrogel, as can be seen, Q has been released steadily and continuously. Based on the results, it can be stated that when oxygen is generated for 13 days, Q is also present in the release medium and can neutralize the free radicals generated during oxygenation. Thus, it can be concluded that the composite scaffold has the sustained capability of oxygen and Q release, which can bring unique biomedical characteristics. This co-delivery is because of SF nature which has an amphiphilic structure that allows the release of low dissolvable biomolecules like Q.

### **3.10. Antibacterial activity (Disc diffusion test)**

MRSA is one of the common microorganisms that cause severe bone infections (Touri et al., 2019). The disc diffusion method with MRSA evaluated the antibacterial activity owing to loaded Q and CPO, which has been a clinically dangerous pathogen in orthopedics (Aleemardani et al., 2020). Figure 6 indicates the inhibition zone of samples (1: Q powder, 2 and 3: GSFQ (hydrogel), and 4: GSFQ-E(SF-1CPO) (composite)) after overnight incubation. Q powder showed a zone of inhibition of 21 mm against MRSA, meaning that the Q has an antibacterial effect in its essence (Amin et al., 2015); hence, it has been chosen as a control. A zone of almost 27 mm related to the GSFQ samples confirms that hydrogels containing Q had an antibacterial activity with sensitivity to MRSA. Also, in GSFQ-E(SF-1CPO), a clear zone of inhibition (approximately 30 mm) was observed; the presence of a breathable patch that contains 1 wt% CPO enhanced the antibacterial activity (Aleemardani et al., 2020). As mentioned, Q continues to grab immense attention because of its various properties, including antioxidant, anti-allergic, anticancer, anti-inflammatory, antidiabetic, antimicrobial, and cardioprotective activities (Memariani et al., 2019).

Therefore, in general, the composite scaffold (GSFQ-E(SF-1CPO)) seems to provide several characteristics that can overcome severe problems and cause improved healing of bone defects.

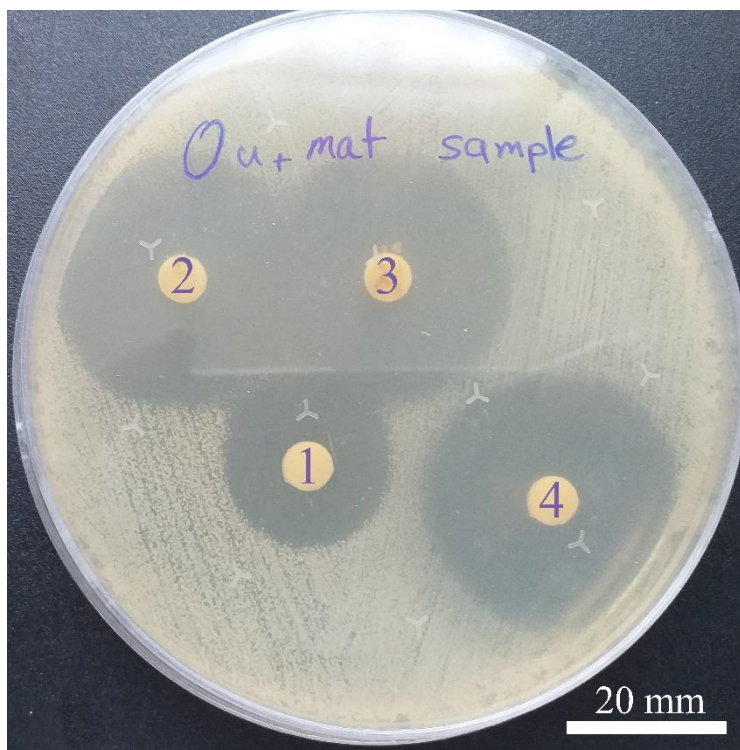


**Figure 6.** MRSA inhibition zone assay of 1: Q powder, 2 and 3: GSFQ (hydrogel), and 4: GSFQ-E(SF-1CPO) (composite) after overnight incubation.

### 3.11. Cellular Assays

#### 3.11.1. Evaluation of Cell Viability in the Vicinity of Quercetin

At the beginning of the study, an MTT test was performed to evaluate the effectiveness of Q. As illustrated in Figure 7A, the cell viability increases significantly with increasing the Q concentration ( $p < 0.01$ ). Q reduces oxidative stress in the microenvironment and affects metabolic and cellular enzymatic activity, indicating that increasing the Q concentration has enhanced cell viability on the first day. According to the literature, the concentration of Q with appropriate

antioxidant properties is in the range of 50-500  $\mu\text{M}$  (Hatahet et al., 2016); therefore, by examining the various amounts on MG-63 cells, the 400  $\mu\text{M}$ , the highest one, not only was not cytotoxic but also improved the cell viability. That is why it was chosen as the optimal concentration in this work.

### 3.11.2. Evaluation of Cell Viability of Scaffolds

The MTT results (both under normoxia and hypoxia) for hydrogels (GSF and GSFQ) and composites (GSF-E(SF-1CPO) and GSFQ-E(SF-1CPO)) are shown in Figures 7B and 7C. According to the results, on day 1, due to the prolonged release of oxygen, cell viability did not increase; however, GSFQ and GSFQ-E (SF-1CPO) contain Q ( $\blacklozenge$ :  $p < 0.05$ ) substantially increased the viability. On day 3, composites improved cell survival due to the onset of oxygen release ( $*$ :  $p < 0.001$ ), notably in GSFQ-E(SF-1CPO), the combined effect of Q and oxygen release led to higher cell viability ( $^{\circ}$ :  $p < 0.01$ ). The highest concentration of dissolved oxygen was on day 6 (Figure 7B); hence, it was expected that the cell viability enhancement would be higher on day 6 than on other days. As can be seen, on this day, composite scaffolds (particularly GSFQ-E(SF-1CPO)) have increased the cellular behaviors compared to the other two days ( $p < 0.0001$ ) remarkably. Moreover, cell survival under hypoxia was investigated and compared with cells cultured at a normal oxygen tension (normoxia) (Figure 7C). Hypoxia led to the decrement in the viability of MG-63 cells, as evidenced by decreased percentages of cell viability ( $p < 0.01$ ). However, the scaffolds containing Q demonstrated substantial improvement in cell viability (%) compared to those without Q ( $\Delta$  and  $\nabla$ :  $p < 0.01$  and  $\#$  and  $\otimes$ :  $p < 0.05$ ). Based on the results, Q promoted cell viability (both in normoxic and hypoxic conditions) with no signs of cytotoxicity, consistent with other studies (Birinci et al., 2020; Chen et al., 2019; Song et al., 2018).

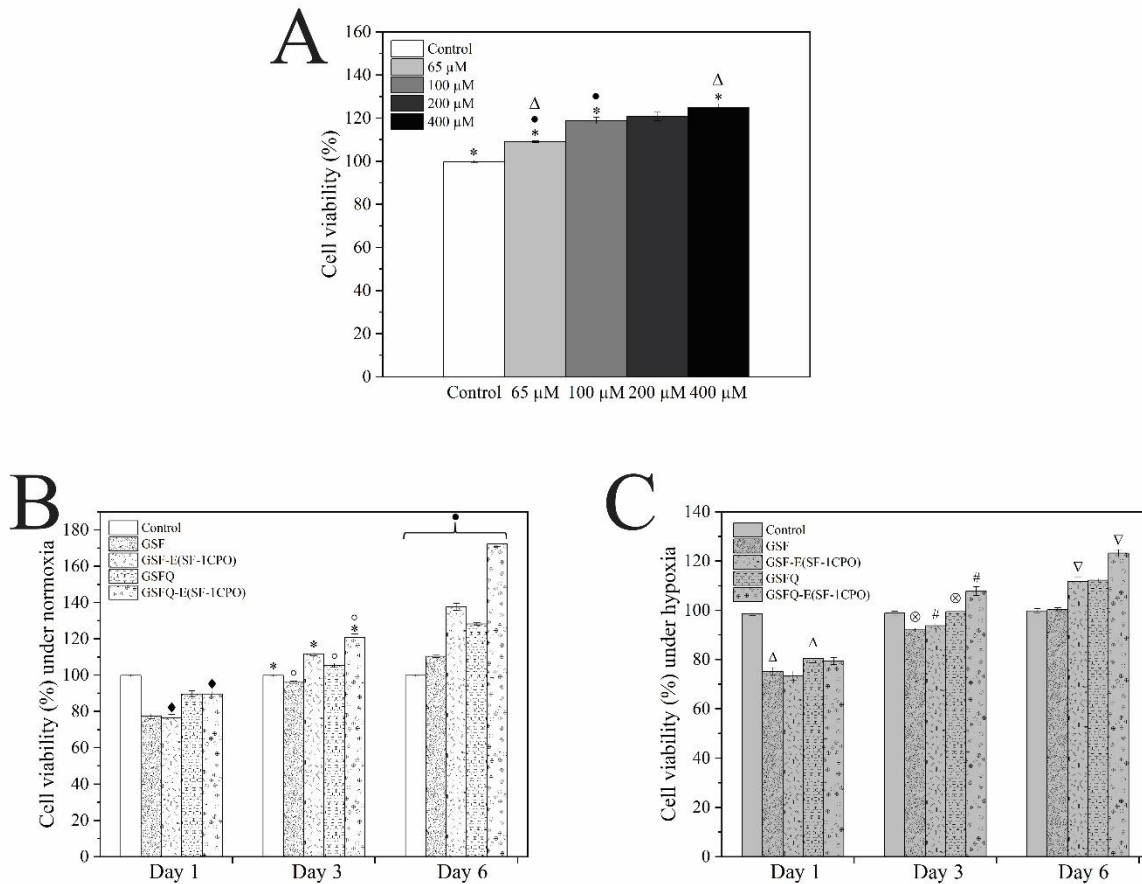


**Figure 7.** Results of the MTT test for (A) different concentrations of Q (\*, • and  $\Delta$ :  $p < 0.01$ ), (B) hydrogels and composites under normoxia ( $\circ$  and  $\bullet$ :  $p < 0.01$ , \*:  $p < 0.001$ , and # and  $\blacklozenge$ :  $p < 0.05$ ) and (C) hydrogels and composites under hypoxia ( $\Delta$  and  $\nabla$ :  $p < 0.01$  and # and  $\otimes$ :  $p < 0.05$ ).

#### 4. Conclusion

This study aimed to develop and evaluate composite scaffolds for the controlled release of oxygen based on SF. SF is a natural polymer that has been selected as a suitable option for CPO encapsulation due to its unique properties (e.g., high biocompatibility, high oxygen permeability, and amphiphilic structure) to fabricate a novel OGB. Burst release and generation of free radicals are substantial challenges for OGBs. A composite structure of hydrogel-fiber-hydrogel and

antioxidant Q were used to meet these two challenges, which are considered other innovations in this field. The composite scaffold can release oxygen and Q for at least 12 days. The results depicted that Q loading led to reasonable antioxidant activity and stabilized oxygen generation. The composite structure resulted in mechanical properties enhancement (mainly because of the incorporation of electrospun fibers into hydrogels). The prepared composite scaffold could be categorized as OGB, antioxidant, and antibacterial, which seems to have adequate potential for tissue engineering applications like bone tissue engineering.

### **Acknowledgment**

The authors would like to express their gratitude to the office of Professional Laboratories and Technology Services in Amirkabir University of Technology (Tehran Polytechnic) for supporting this research under grant number 1400-0506. We are thankful for Dr. Chris Holland's comments, which helped us improve our research paper.

### **Conflicts of Interest**

There are no conflicts to declare.

### **Author Contributions**

Mina Aleemardani conducted the experiments, validated and analyzed data, investigated and drafted the manuscript. Atefeh Solouk supervised the research, administered the project and critically revised the manuscript. Somaye Akbari and Mohammad Moeini participated in the conceptualization, methodology, reviewing and editing.

## References

- Abdi SIH, Ng SM, Lim JO. 2011. An enzyme-modulated oxygen-producing micro-system for regenerative therapeutics. *Int. J. Pharm.* **409**:203–205.
- Agarwal T, Kazemi S, Costantini M, Perfeito F, Correia CR, Gaspar V, Montazeri L, De Maria C, Mano JF, Vosough M. 2021. Oxygen releasing materials: towards addressing the hypoxia-related issues in tissue engineering. *Mater. Sci. Eng. C*:111896.
- Aleemardani M, Bagher Z, Farhadi M, Chahsetareh H, Najafi R, Eftekhari B, Seifalian A. 2021a. Can Tissue Engineering Bring Hope to the Development of Human Tympanic Membrane? *Tissue Eng. Part B Rev.*
- Aleemardani M, Solouk A, Akbari S, Dehghan MM, Moeini M. 2020. Silk-derived oxygen-generating electrospun patches for enhancing tissue regeneration: Investigation of calcium peroxide role and its effects in controlled oxygen delivery. *Materialia*:100877.
- Aleemardani M, Trikić MZZ, Green NHH, Claeysens F. 2021b. The Importance of Mimicking Dermal-Epidermal Junction for Skin Tissue Engineering: A Review. *Bioengineering* **8**:148.
- Aleemardani M, Zare P, Seifalian A, Bagher Z, Seifalian AM. 2021c. Graphene-Based Materials Prove to Be a Promising Candidate for Nerve Regeneration Following Peripheral Nerve Injury. *Biomedicines* **10**:73.
- Alemdar N, Leijten J, Camci-Unal G, Hjortnaes J, Ribas J, Paul A, Mostafalu P, Gaharwar AK, Qiu Y, Sonkusale S. 2016. Oxygen-generating photo-cross-linkable hydrogels support cardiac progenitor cell survival by reducing hypoxia-induced necrosis. *ACS Biomater. Sci. Eng.* **3**:1964–1971.
- Alizadeh SR, Ebrahimzadeh MA. 2021. Quercetin derivatives: Drug design, development, and biological activities, a review. *Eur. J. Med. Chem.*:114068.
- Amer SS, Mamdouh W, Nasr M, ElShaer A, Polycarpou E, Abdel-Aziz RTA, Sammour OA.

2021. Quercetin loaded cosm-nutraceutical electrospun composite nanofibers for acne alleviation: Preparation, characterization and experimental clinical appraisal. *Int. J. Pharm.*:121309.
- Amin MU, Khurram M, Khattak B, Khan J. 2015. Antibiotic additive and synergistic action of rutin, morin and quercetin against methicillin resistant *Staphylococcus aureus*. *BMC Complement. Altern. Med.* **15**:59.
- An JA, Kang J II, Park KM, Park KD. 2019. Calcium peroxide-mediated oxygen supply for improved coating efficiency of bio-inspired catecholamine. *J. Ind. Eng. Chem.* **80**:795–801.
- Ashammakhi N, Darabi MA, Kehr NS, Erdem A, Hu S, Dokmeci MR, Nasr AS, Khademhosseini A. 2019a. Advances in Controlled Oxygen Generating Biomaterials for Tissue Engineering and Regenerative Therapy. *Biomacromolecules*.
- Ashammakhi N, Hasan A, Kaarela O, Byambaa B, Sheikhi A, Gaharwar AK, Khademhosseini A. 2019b. Advancing frontiers in bone bioprinting. *Adv. Healthc. Mater.* **8**:1801048.
- Bai X, Lü S, Cao Z, Gao C, Duan H, Xu X, Sun L, Gao N, Feng C, Liu M. 2016. Self-reinforcing injectable hydrogel with both high water content and mechanical strength for bone repair. *Chem. Eng. J.* **288**:546–556.
- Birinci Y, Niazi JH, Aktay-Çetin O, Basaga H. 2020. Quercetin in the form of a nano-antioxidant (QTiO<sub>2</sub>) provides stabilization of quercetin and maximizes its antioxidant capacity in the mouse fibroblast model. *Enzyme Microb. Technol.*:109559.
- Buser Z, Brodke DS, Youssef JA, Meisel H-J, Myhre SL, Hashimoto R, Park J-B, Yoon ST, Wang JC. 2016. Synthetic bone graft versus autograft or allograft for spinal fusion: a systematic review. *J. Neurosurg. Spine* **25**:509–516.
- Caddeo C, Gabriele M, Fernández-Busquets X, Valenti D, Fadda AM, Pucci L, Manconi M.

2019. Antioxidant activity of quercetin in Eudragit-coated liposomes for intestinal delivery. *Int. J. Pharm.* **565**:64–69.
- Camci-Unal G, Alemdar N, Annabi N, Khademhosseini A. 2013. Oxygen-releasing biomaterials for tissue engineering. *Polym. Int.* **62**:843–848.
- Catauro M, Papale F, Bollino F, Piccolella S, Marciano S, Nocera P, Pacifico S. 2015. Silica/quercetin sol–gel hybrids as antioxidant dental implant materials. *Sci. Technol. Adv. Mater.*
- Chen S, Zhu L, Wen W, Lu L, Zhou C, Luo B. 2019. Fabrication and evaluation of 3D printed poly (L-lactide) scaffold functionalized with quercetin-polydopamine for bone tissue engineering. *ACS Biomater. Sci. Eng.* **5**:2506–2518.
- Choi Y, Park MH, Lee K. 2020. Injectable thermoresponsive hydrogel/nanofiber hybrid scaffolds inducing human adipose-derived stem cell chemotaxis. *J. Ind. Eng. Chem.* **82**:89–97.
- Cirillo G, Iemma F. 2012. Antioxidant Polymers: Synthesis, Properties, and Applications. John Wiley & Sons.
- Coronel MM, Liang J-P, Li Y, Stabler CL. 2019. Oxygen generating biomaterial improves the function and efficacy of beta cells within a macroencapsulation device. *Biomaterials* **210**:1–11.
- Daneshmandi L, Laurencin CT. Regenerative Engineered Vascularized Bone Mediated by Calcium Peroxide. *J. Biomed. Mater. Res. Part A.*
- Diez-Echave P, Ruiz-Malagón AJ, Molina-Tijeras JA, Hidalgo-García L, Vezza T, Cenis-Cifuentes L, Rodríguez-Sojo MJ, Cenis JL, Rodríguez-Cabezas ME, Rodríguez-Nogales A. 2021. Silk fibroin nanoparticles enhance quercetin immunomodulatory properties in DSS-

- induced mouse colitis. *Int. J. Pharm.* **606**:120935.
- Farling S, Straube TL, Vesel TP, Bottenus N, Klitzman B, Cheifetz IM, Deshusses MA. 2021. Development of a novel intravascular oxygenator catheter: Oxygen mass transfer properties across nonporous hollow fiber membranes. *Biotechnol. Bioeng.* **118**:345–356.
- Farokhi M, Aleemardani M, Solouk A, Mirzadeh H, Teuschl AH, Redl H. 2021. Crosslinking strategies for silk fibroin hydrogels: promising biomedical materials. *Biomed. Mater.* **16**:22004. <http://dx.doi.org/10.1088/1748-605X/abb615>.
- Farokhi M, Mottaghitalab F, Fatahi Y, Khademhosseini A, Kaplan DL. 2018. Overview of silk fibroin use in wound dressings. *Trends Biotechnol.* **36**:907–922.
- Farzaneh Z, Abbasalizadeh S, Asghari-Vostikolaee M, Alikhani M, Cabral JMS, Baharvand H. 2020. Dissolved oxygen concentration regulates human hepatic organoid formation from pluripotent stem cells in a fully controlled bioreactor. *Biotechnol. Bioeng.* **117**:3739–3756.
- Fernández-García L, Marí-Buyé N, Barios JA, Madurga R, Elices M, Pérez-Rigueiro J, Ramos M, Guinea G V, González-Nieto D. 2016. Safety and tolerability of silk fibroin hydrogels implanted into the mouse brain. *Acta Biomater.* **45**:262–275.
- Gholipourmalekabadi M, Zhao S, Harrison BS, Mozafari M, Seifalian AM. 2016. Oxygen-generating biomaterials: a new, viable paradigm for tissue engineering? *Trends Biotechnol.* **34**:1010–1021.
- Gori M, Giannitelli SM, Zanca A, Mozetic P, Trombetta M, Merendino N, Rainer A. 2021. Quercetin and hydroxytyrosol as modulators of hepatic steatosis: A NAFLD-on-a-chip study. *Biotechnol. Bioeng.* **118**:142–152.
- Griffin KS, Davis KM, McKinley TO, Anglen JO, Chu T-MG, Boerckel JD, Kacena MA. 2015. Evolution of bone grafting: bone grafts and tissue engineering strategies for vascularized

- bone regeneration. *Clin. Rev. Bone Miner. Metab.* **13**:232–244.
- Guaccio A, Guarino V, Perez MAA, Cirillo V, Netti PA, Ambrosio L. 2011. Influence of electrospun fiber mesh size on hMSC oxygen metabolism in 3D collagen matrices: Experimental and theoretical evidences. *Biotechnol. Bioeng.* **108**:1965–1976.
- Guziewicz N, Best A, Perez-Ramirez B, Kaplan DL. 2011. Lyophilized silk fibroin hydrogels for the sustained local delivery of therapeutic monoclonal antibodies. *Biomaterials* **32**:2642–2650.
- Harrass K, Krüger R, Möller M, Albrecht K, Groll J. 2013. Mechanically strong hydrogels with reversible behaviour under cyclic compression with MPa loading. *Soft Matter* **9**:2869–2877.
- Hatahet T, Morille M, Hommoss A, Devoisselle JM, Müller RH, Bégu S. 2016. Quercetin topical application, from conventional dosage forms to nanodosage forms. *Eur. J. Pharm. Biopharm.* **108**:41–53.
- Jang SR, Kim JI, Park CH, Kim CS. 2020. The controlled design of electrospun PCL/silk/quercetin fibrous tubular scaffold using a modified wound coil collector and L-shaped ground design for neural repair. *Mater. Sci. Eng. C*:110776.
- Kagawa Y, Matsuura K, Shimizu T, Tsuneda S. 2015. Direct measurement of local dissolved oxygen concentration spatial profiles in a cell culture environment. *Biotechnol. Bioeng.* **112**:1263–1274.
- Kang YB, Eo J, Bulutoglu B, Yarmush ML, Usta OB. 2020. Progressive hypoxia-on-a-chip: An in vitro oxygen gradient model for capturing the effects of hypoxia on primary hepatocytes in health and disease. *Biotechnol. Bioeng.* **117**:763–775.
- Karageorgiou V, Kaplan D. 2005. Porosity of 3D biomaterial scaffolds and osteogenesis. *Biomaterials* **26**:5474–5491.

- Khorasani MT, Joorabloo A, Moghaddam A, Shamsi H, MansooriMoghadam Z. 2018. Incorporation of ZnO nanoparticles into heparinised polyvinyl alcohol/chitosan hydrogels for wound dressing application. *Int. J. Biol. Macromol.* **114**:1203–1215.
- Khorshidi S, Karimi-Soflou R, Karkhaneh A. 2021. A hydrogel/particle composite with a gradient of oxygen releasing microparticle for concurrent osteogenic and chondrogenic differentiation in a single scaffold. *Colloids Surfaces B Biointerfaces* **207**:112007.
- Khorshidi S, Karkhaneh A. 2021. A hydrogel/particle composite with gradient in oxygen releasing microparticle for oxygenation of the cartilage-to-bone interface: Modeling and experimental viewpoints. *Mater. Sci. Eng. C* **118**:111522.
- Khorshidi S, Karkhaneh A, Bonakdar S. 2019. Fabrication of amine-decorated non-spherical microparticles with calcium peroxide cargo for controlled release of oxygen. *J. Biomed. Mater. Res. Part A*.
- Li Z, Song J, Zhang J, Hao K, Liu L, Wu B, Zheng X, Xiao B, Tong X, Dai F. 2020. Topical application of silk fibroin-based hydrogel in preventing hypertrophic scars. *Colloids Surfaces B Biointerfaces* **186**:110735.
- Lobo V, Patil A, Phatak A, Chandra N. 2010. Free radicals, antioxidants and functional foods: Impact on human health. *Pharmacogn. Rev.* **4**:118.
- Loh QL, Choong C. 2013. Three-dimensional scaffolds for tissue engineering applications: role of porosity and pore size. *Tissue Eng. Part B Rev.* **19**:485–502.
- Lozano-Pérez AA, Rivero HC, Hernández M del CP, Pagán A, Montalbán MG, VÍllora G, Cénis JL. 2017. Silk fibroin nanoparticles: Efficient vehicles for the natural antioxidant quercetin. *Int. J. Pharm.* **518**:11–19.
- Lv X, Li Z, Chen S, Xie M, Huang J, Peng X, Yang R, Wang H, Xu Y, Feng C. 2016. Structural

- and functional evaluation of oxygenating keratin/silk fibroin scaffold and initial assessment of their potential for urethral tissue engineering. *Biomaterials* **84**:99–110.
- Matsumoto A, Chen J, Collette AL, Kim U-J, Altman GH, Cebe P, Kaplan DL. 2006. Mechanisms of silk fibroin sol– gel transitions. *J. Phys. Chem. B* **110**:21630–21638.
- Memariani H, Memariani M, Ghasemian A. 2019. An overview on anti-biofilm properties of quercetin against bacterial pathogens. *World J. Microbiol. Biotechnol.* **35**:143.
- Milanezi FG, Meireles LM, de Christo Scherer MM, de Oliveira JP, da Silva AR, de Araujo ML, Endringer DC, Fronza M, Guimarães MCC, Scherer R. 2019. Antioxidant, antimicrobial and cytotoxic activities of gold nanoparticles capped with quercetin. *Saudi Pharm. J.* **27**:968–974.
- Mohamed S, Shamaz BH. 2015. Bone Tissue Engineering and Bony Scaffolds. *Int J Dent Oral Heal* **1**:1–15.
- Nejati S, Soflou RK, Khorshidi S, Karkhaneh A. 2020. Development of an oxygen-releasing electroconductive in-situ crosslinkable hydrogel based on oxidized pectin and grafted gelatin for tissue engineering applications. *Colloids Surfaces B Biointerfaces*:111347.
- Pathi B, Kinsey ST, Locke BR. 2013. Oxygen control of intracellular distribution of mitochondria in muscle fibers. *Biotechnol. Bioeng.* **110**:2513–2524.
- Pedraza E, Coronel MM, Fraker CA, Ricordi C, Stabler CL. 2012. Preventing hypoxia-induced cell death in beta cells and islets via hydrolytically activated, oxygen-generating biomaterials. *Proc. Natl. Acad. Sci.* **109**:4245–4250.
- Phelps EA, García AJ. 2010. Engineering more than a cell: vascularization strategies in tissue engineering. *Curr. Opin. Biotechnol.* **21**:704–709.
- Pritchard EM, Kaplan DL. 2011. Silk fibroin biomaterials for controlled release drug delivery.

- Expert Opin. Drug Deliv.* **8**:797–811.
- Reimers K, Liebsch C, Radtke C, Kuhbier JW, Vogt PM. 2015. Silks as scaffolds for skin reconstruction. *Biotechnol. Bioeng.* **112**:2201–2205.
- Samal SK, Dash M, Chiellini F, Wang X, Chiellini E, Declercq HA, Kaplan DL. 2014. Silk/chitosan biohybrid hydrogels and scaffolds via green technology. *RSC Adv.* **4**:53547–53556.
- Sammi A, Mahapatra S, Kumar R, Chandra P. 2021. Nano-Bio-engineered Silk Matrix based Devices for Molecular Bioanalysis. *Biotechnol. Bioeng.*
- Sarker B, Papageorgiou DG, Silva R, Zehnder T, Gul-E-Noor F, Bertmer M, Kaschta J, Chrissafis K, Detsch R, Boccaccini AR. 2014. Fabrication of alginate–gelatin crosslinked hydrogel microcapsules and evaluation of the microstructure and physico-chemical properties. *J. Mater. Chem. B* **2**:1470–1482.
- Sayyad N, Maji R, Omolo CA, Ibrahim UH, Pathan TK, Devnarain N, Karpoormath R, Dhawan S, Obakachi VA, Merugu SR. 2021. Development of niosomes for encapsulating captopril-quercetin prodrug to combat hypertension. *Int. J. Pharm.* **609**:121191.
- Seib FP, Pritchard EM, Kaplan DL. 2013. Self-assembling doxorubicin silk hydrogels for the focal treatment of primary breast cancer. *Adv. Funct. Mater.* **23**:58–65.
- Selvaraj S, Fathima NN. 2017. Fenugreek Incorporated Silk Fibroin Nanofibers □ A Potential Antioxidant Scaffold for Enhanced Wound Healing. *ACS Appl. Mater. Interfaces* **9**:5916–5926.
- Sheng F, Chow PS, Hu J, Cheng S, Guo L, Dong Y. 2020. Preparation of quercetin nanorod/microcrystalline cellulose formulation via fluid bed coating crystallization for dissolution enhancement. *Int. J. Pharm.* **576**:118983.

- Shiekh PA, Singh A, Kumar A. 2018. Engineering bioinspired antioxidant materials promoting cardiomyocyte functionality and maturation for tissue engineering application. *ACS Appl. Mater. Interfaces* **10**:3260–3273.
- Song JE, Tripathy N, Lee DH, Park JH, Khang G. 2018. Quercetin inlaid silk fibroin/hydroxyapatite scaffold promotes enhanced osteogenesis. *ACS Appl. Mater. Interfaces* **10**:32955–32964.
- de Sousa Araújo E, Stocco TD, de Sousa GF, Afewerki S, Marciano FR, Corat MAF, de Paula MMM, Verde TFCL, Silva MCM, Lobo AO. 2021. Oxygen-generating microparticles in chondrocytes-laden hydrogels by facile and versatile click chemistry strategy. *Colloids Surfaces B Biointerfaces* **205**:111850.
- Steg H, Buizer AT, Woudstra W, Veldhuizen AG, Bulstra SK, Grijpma DW, Kuijer R. 2017. Oxygen-releasing poly (trimethylene carbonate) microspheres for tissue engineering applications. *Polym. Adv. Technol.* **28**:1252–1257.
- Suvarnapathaki S, Nguyen MA, Goulopoulos AA, Lantigua D, Camci-Unal G. 2021a. Engineering calcium peroxide based oxygen generating scaffolds for tissue survival. *Biomater. Sci.* **9**:2519–2532.
- Suvarnapathaki S, Wu X, Zhang T, Nguyen MA, Goulopoulos AA, Wu B, Camci-Unal G. 2021b. Oxygen generating scaffolds regenerate critical size bone defects. *Bioact. Mater.*
- Touri M, Moztafzadeh F, Abu Osman NA, Dehghan MM, Brouki Milan P, Farzad-Mohajeri S, Mozafari M. 2020. Oxygen-releasing scaffolds for accelerated bone regeneration. *ACS Biomater. Sci. Eng.*
- Touri M, Moztafzadeh F, Osman NAA, Dehghan MM, Mozafari M. 2019. Optimisation and biological activities of bioceramic robocast scaffolds provided with an oxygen-releasing

- coating for bone tissue engineering applications. *Ceram. Int.* **45**:805–816.
- Tran HDN, Park KD, Ching YC, Huynh C, Nguyen DH. 2020. A comprehensive review on polymeric hydrogel and its composite: Matrices of choice for bone and cartilage tissue engineering. *J. Ind. Eng. Chem.*
- Vériter S, Gianello P, Dufrane D. 2013. Bioengineered sites for islet cell transplantation. *Curr. Diab. Rep.* **13**:745–755.
- Wang J, Su Q, Lv Q, Cai B, Xiaohalati X, Wang G, Wang Z, Wang L. 2021. Oxygen-Generating Cyanobacteria Powered by Upconversion-Nanoparticles-Converted Near-Infrared Light for Ischemic Stroke Treatment. *Nano Lett.*
- Wang W, Sun C, Mao L, Ma P, Liu F, Yang J, Gao Y. 2016. The biological activities, chemical stability, metabolism and delivery systems of quercetin: A review. *Trends Food Sci. Technol.* **56**:21–38.
- Watanabe M, Bhawal UK, Takemoto S, Nishiyama N, Nakahara Y, Tatematsu K, Sezutsu H, Kuwabara N, Minamisawa T, Shiba K. 2021. Bio-functionalized titanium surfaces with modified silk fibroin carrying titanium binding motif to enhance the ossific differentiation of MC3T3-E1. *Biotechnol. Bioeng.*
- Xu S, Deng L, Zhang J, Yin L, Dong A. 2016. Composites of electrospun-fibers and hydrogels: A potential solution to current challenges in biological and biomedical field. *J. Biomed. Mater. Res. Part B Appl. Biomater.* **104**:640–656.
- Yadav S, Mehrotra GK, Bhartiya P, Singh A, Dutta PK. 2020. Preparation, physicochemical and biological evaluation of quercetin based chitosan-gelatin film for food packaging. *Carbohydr. Polym.* **227**:115348.
- Yodmuang S, McNamara SL, Nover AB, Mandal BB, Agarwal M, Kelly T-AN, Chao PG, Hung

C, Kaplan DL, Vunjak-Novakovic G. 2015. Silk microfiber-reinforced silk hydrogel composites for functional cartilage tissue repair. *Acta Biomater.* **11**:27–36.

Zare P, Aleemardani M, Seifalian A, Bagher Z, Seifalian AM. 2021. Graphene Oxide: Opportunities and Challenges in Biomedicine. *Nanomaterials* **11**:1083.

# Graphical Abstract (Table of Content Graphic)

